INTERNATIONAL JOURNAL OF HYDROGEN ENERGY 34 (2009) 8339–8351

Available at www.sciencedirect.com

ScienceDirect

journal homepage: www.elsevier.com/locate/he

Numerical and experimental analysis of NO emissions from a lab-scale burner fed with hydrogen-enriched fuels and operating in MILD combustion

C. Galletti[a,*], A. Parente[a], M. Derudi[b], R. Rota[b], L. Tognotti[a]

[a]Dipartimento di Ingegneria Chimica, Chimica Industriale e Scienza dei Materiali, Università di Pisa, via Diotisalvi 2, I-56126 Pisa, Italy
[b]Politecnico di Milano, Dipartimento di Chimica, Materiali e Ingegneria Chimica "G. Natta"/CIIRCO, Milano, Italy

ARTICLE INFO

Article history:
Received 29 April 2009
Received in revised form
23 July 2009
Accepted 26 July 2009
Available online 12 August 2009

Keywords:
Flameless combustion
Hydrogen
Combustion model
Kinetic mechanism
NO_x
Computational fluid dynamics

ABSTRACT

An experimental and computational investigation of a lab-scale burner, which can operate in both flame and MILD combustion conditions and is fed with methane and a methane/hydrogen mixture (hydrogen content of 60% by vol.), is carried out. The modelling results indicate the need of a proper turbulence/chemistry interaction treatment and rather detailed kinetic mechanisms to capture MILD combustion features, especially in presence of hydrogen. Despite these difficulties, Computational Fluid Dynamics results to be very useful, as for instance it allows evaluating the internal recirculation degree in the burner, a parameter which is otherwise difficult to be determined. Moreover the model helps interpreting experimental evidences: for instance the modelling results indicate that in presence of hydrogen the NNH and N_2O intermediate routes are the dominant formation pathways for the MILD combustion conditions investigated.

1. Introduction

MILD combustion [1,2] also called Flameless Oxidation (FO) [3] or High Temperature Air Combustion (HiTAC) [4], is a combustion technology able to strongly control pollutants production, in particular that of CO and NO_x, limiting their formation directly inside the furnace.

MILD combustion is generally achieved through a massive recirculation of exhaust gases in the reaction region, which allows diluting the fresh gases before reaction can occur. Besides the reactants have to be heated up above their self-ignition temperature, allowing the combustion process to be sustained. The oxidation process is distributed across a relatively large volume rather than restricted to a flame front, thus reducing temperature peaks and NO formation via thermal mechanism. Soot formation can be also inhibited, due to the lean conditions, low temperatures and the large CO_2 concentration in the exhausts.

Subsequently, MILD combustion burners appear well suited for those industrial processes that require a high and homogeneous temperature distribution within the combustion chamber (e.g., in the glass and ceramic industry, in steel thermal treatments). For these processes, energy recovery represents a primary issue to ensure acceptable energy efficiency; consequently, the use of MILD combustion is considered to be particularly beneficial and constitutes an accepted technology.

However, the increasing interest in MILD combustion is due to the fact that it allows a large fuel flexibility, as it seems to be suited for low-calorific value fuels [5,6], high-calorific

* *Corresponding author*. Tel.: +39 050 2217897; fax: +39 050 2217866.
E-mail address: chiara.galletti@ing.unipi.it (C. Galletti).
0360-3199/$ – see front matter © 2009 Professor T. Nejat Veziroglu. Published by Elsevier Ltd. All rights reserved.
doi:10.1016/j.ijhydene.2009.07.095

Nomenclature and units

$\lvert\tilde{E}/\overline{y}_e\rvert_{avg}$	average error metrics normalized with respect to the measured value
F	volumetric flow rate, $m^3\,s^{-1}$
k	turbulent kinetic energy, $m^2\,s^{-2}$
k_2k_{p1}	product of reaction constants, $m^3\,mol^{-1}\,s^{-1}$
k_v	dilution ratio
$\dot{m}$	mass flow rate, $kg\,s^{-1}$
p	grid order of convergence
r	radial coordinate, m
R	radius of the combustion chamber, m
R_A	aerodynamic recirculation ratio
T	temperature, K
v	axial velocity, $m\,s^{-1}$
x	axial coordinate, m
X	molar fraction
X_H	mole fraction of H atoms
$\overline{y}_e$	mean measurement of variable y
y_m	predicted value of variable y
Y	mass fraction
Y^*	fine structures mass fraction
$\tilde{Y}$	mean mass fraction
Y^0	surrounding state mass fraction
$\overline{w}$	mean reaction rate, $kg\,m^{-3}\,s^{-1}$

Greek symbols

ρ	density, $kg\,m^{-3}$
$\overline{\rho}$	density of the mixture, $kg\,m^{-3}$
ε	kinetic energy dissipation rate, $m^2\,s^{-3}$
υ	kinematic viscosity, $m^2\,s^{-1}$
γ_λ	mass fraction of the fine structures
τ^*	mean residence time in the fine structures, s

Subscripts

A	air
AI	primary air
AII	secondary air
C	center of recirculation loop
E	recirculating exhaust gases
F	fuel
I	inert
in	inlet gases
k	species index
m	mixed value, referred to the mixing process of fresh and flue gases

Abbreviations

ED	eddy dissipation model
EDC	eddy dissipation concept
FR	finite rate chemistry model
HiTAC	high temperature air combustion
MILD	moderate or intense low oxygen dilution
PDF	probability density function
PSR	perfectly stirred reactor
WSGG	weighted sum of gray gases

industrial wastes, as well as in presence of hydrogen. In this latter case, MILD combustion constitutes an interesting choice as H_2 as a fuel shows specific properties (high laminar flame speed, high adiabatic flame temperature and heating value, high reactivity, etc. [7]) which make conventional burners unsuited. Recently Derudi et al. [8] showed that MILD combustion can be successfully applied for the utilization of the coke oven gas (COG), which is a byproduct of the coke-making process and is typically constituted by a CH_4/H_2 mixture with a composition of 40/60% by vol.; these experimental results have been recently confirmed in a numerical kinetic study aimed to simulate with a network of perfectly stirred reactors the MILD combustion of different hydrogen–methane mixtures [9]. In addition, Sabia et al. [10] demonstrated how the addition of small amounts of hydrogen has a beneficial influence in terms of reduction of thermo-kinetic instabilities observed in methane MILD combustion.

In this work, experimental runs have been carried out in a lab-scale burner fed with methane and methane/hydrogen mixtures in order to assess the MILD combustion regime and measure burner performances, especially in terms of NO_x emissions.

The results from the experimental campaign, i.e. flue gases composition and some temperatures in the burner, have been compared with Computational Fluid Dynamics (CFD) simulations, performed for both flame and MILD conditions, in order to gain insight into the conditions at which the burner is operated.

Particular attention has been devoted to the modelling of turbulence/chemistry interaction, as this constitutes a key aspect for the accurate modelling of MILD combustion. In conventional flames, most of the times it can be assumed that the oxidation processes occur nearly instantaneously, and that turbulent mixing governs the reaction rate (following the so called ‘‘mixed is burnt approach’’). Conversely, in MILD combustion the low reactants concentration, which characterizes the reaction region, leads to an increase of the chemical timescales; on the other hand the enhanced turbulence levels due to exhaust gases recirculation reduce the turbulent mixing timescales. Consequently, the turbulent and chemical timescales become similar and it is a generalised opinion that the Damköhler number (turbulent to chemical timescale ratio) approaches unity. In such conditions the numerical modelling should take into account both mixing and chemistry, becoming a very challenging task.

Actually, the modelling requisites for MILD combustion in terms of both turbulence/chemistry interaction treatment (through a combustion model) and extent of the kinetic mechanisms adopted, have not been defined yet, albeit recently several works on MILD combustion modelling have been published, e.g., [11–14].

Moreover, in the present work many efforts have been spent to model the NO formation process, in order to explain and interpret the experimental NO emissions. Because of the low process temperatures and low fluctuations characterizing MILD combustion, the thermal NO formation route (usually

the dominant one in conventional flames) is suppressed [15]. Consequently, the CFD model should include other routes such as Fenimore's prompt and the N_2O intermediate route (which is a low-temperature pathway).

Moreover, the presence of H_2 in the fuel may promote NO formation through the NNH intermediate mechanism:

$$N_2 + H \leftrightarrow NNH \quad (1)$$

$$NNH + O \leftrightarrow NH + NO \quad (2)$$

The direct oxidation of NNH to NO was firstly proposed by Bozzelli and Dean [16] and lately confirmed by Hayhurst and Hutchinson [17], who performed measurements of NO_x in a laminar premixed flat CH_4/H_2 flame. Results showed that NO_x concentration was too high to be explained entirely by the Zeldovich mechanism. The inclusion of the NNH route proposed by Bozzelli and Dean [16] gave reasonable good agreement with experimental observations.

Konnov et al. [18] performed numerical simulations of NO formation during hydrogen combustion in well stirred reactors. Numerical results were compared to experiments carried out in the temperature range of 1500–2200 K. The authors observed that the NNH route represents the dominant source of NO at 1500 K, not only in rich conditions [19], but also in lean mixtures and at stoichiometric. Rørtveit et al. [20] investigated the effect of diluents addition on NO_x formation in hydrogen laminar counterflow flames. The authors also found significant contributions of the N_2O and NNH mechanisms on the overall NO production at low temperatures (~1800 K). They also observed a slight temperature dependency of such mechanisms, differently from the thermal mechanism, which rapidly became the most significant contribution to NO at temperatures around 2100 K. Guo et al. [21] investigated the effect of hydrogen addition to ultra-lean counterflow CH_4/air premixed flames on the flammability limits and NO_x emissions. Results showed that N_2O and NNH routes played a major role on the NO formation, while the thermal and prompt mechanism resulted in minor contributions, due to the lean conditions and the low temperatures. Gauthier et al. [22] studied the flame structure and nitrogen oxides formation in lean porous premixed combustion of natural gas/hydrogen blends; for the investigated conditions they found that the NNH, N_2O and prompt pathways are the most important routes involved in NO formation. Löffler et al. [19] recently developed a new simplified reaction scheme to model NO_x formation in natural gas combustion. The model was tested in a wide range of conditions and compared to more detailed kinetic schemes [23] under premixed plug-flow reactor conditions. Results confirmed that NO formation is dominated by the thermal mechanism at temperatures higher than 1800 K. At lower temperatures and with increasing oxygen availability, the N_2O mechanism gave significant contribution, due to the increased O radical concentration. On the contrary, NNH dominated below 1600 K and in fuel rich conditions, when the concentration of H radicals is higher. Skottene and Rian [24] compared different detailed mechanisms for the prediction of NO_x formation in laminar hydrogen flames and turbulent hydrogen jet flames. Results showed the important role of the NNH pathway in NO formation for all the flames investigated.

2. Experimental apparatus

The laboratory-scale equipment has been extensively described in detail elsewhere [8,25,26]; only the main features of the burner, sketched in Fig. 1, are here summarized. It is a vertical quartz reactor constituted by two sections: the air pre-heater and the combustion chamber. Both sections of the burner are enclosed within refractory insulated electrical ovens. The lower one provides air preheating up to 1300 °C, simulating a regenerative heat exchanger, while the upper one is used only to limit heat losses from the combustion chamber. The combustion chamber is cylindrical with a radius of 0.025 m and a length of 0.33 m. The burner core is constituted by a single high-velocity nozzle with an inner diameter of 0.003 m located at the bottom of the combustion chamber, into which the fuel is fed perpendicularly through a capillary pipe. Inside the nozzle body, fuel and combustion air are only partly premixed before the reactants stream enters the combustion chamber; however no combustion reaction takes place (as experimentally verified) due to the designed small diameter of the feeding pipe and the short residence time. In this way a high-velocity jet is achieved, leading to a large entrainment of burnt gases. Moreover, in addition to such an internal recycle, an external exhausts recycle can be simulated by vitiating the combustion air with an inert gas, such as nitrogen. The burner is also provided by a secondary inlet for the combustion air, located on the bottom of the preheating section, used during the system start-up [8] in conventional stabilized flame conditions before switching to MILD conditions. The exhaust gases exit from one central and three eccentric outlets placed on the top of the combustion chamber.

This small-scale experimental setup allows changing independently the values of those parameters that are relevant for MILD conditions achievement, namely: jet velocity, combustion chamber temperature and dilution ratio.

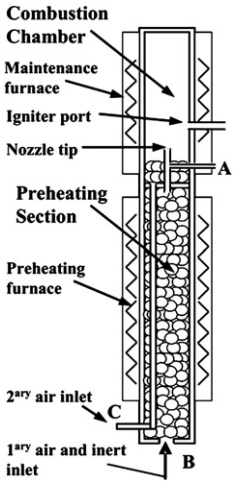

Fig. 1 – Sketch of the lab-scale MILD burner.

The dilution ratio k_v takes into account both the internal recirculation of exhaust gases as well as the dilution due to a possible inert gas addition to the feeding stream. It is defined as:

$$k_v = \frac{\dot{m}_E - \dot{m}_{AII}}{\dot{m}_A + \dot{m}_F} \quad (3)$$

where $\dot{m}_A$ is the sum of the primary air mass flow rate, $\dot{m}_{AI}$, fed with the fuel through the high-velocity nozzle, and the secondary air mass flow rate, $\dot{m}_{AII}$, whereas $\dot{m}_E$ and $\dot{m}_F$ denote the mass flow rates of recirculated flue gases and fuel, respectively. An aerodynamic recirculation ratio, R_A, can be introduced to compare the recirculated and inlet (air and fuel) mass flow rates:

$$R_A = \frac{\dot{m}_E + \dot{m}_{AII}}{\dot{m}_{AI} + \dot{m}_F + \dot{m}_I} \quad (4)$$

Eq. (4) has been derived assuming that the secondary air is completely entrained by the jet issuing into the combustion chamber. Substituting Eq. (4) in Eq. (3), the following expression for k_v is recovered:

$$k_v = \frac{R_A(\dot{m}_{AI} + \dot{m}_F + \dot{m}_I) - \dot{m}_{AII}}{\dot{m}_A + \dot{m}_F} \quad (5)$$

where $\dot{m}_I$ represents the mass flow rate of the dilution inert, i.e. N_2, introduced to simulate external flue gas recirculation.

Concerning pollutants emissions, a quartz probe is used to sample part of the gases at the exhaust exit; the sampled gas is then dried and analyzed by means of an on-line gas analyzer (Horiba PG-250), which measures the concentrations of NO_x, O_2, CO and CO_2, while temperatures at three different positions inside the combustion chamber (in particular one close to the exhaust exit) are continuously monitored.

Various operating conditions, ranging from stable flame to stable MILD combustion (through a transition region where MILD conditions cannot be steadily sustained even though reactants are quite diluted and furnace temperature are high enough) have been investigated, as summarized in Table 1. Commonly the MILD regime is identified by flame disappearing, reduction of temperature gradients inside the furnace, and a decrease of noise; this means a strong decrease of NO_x and CO emissions, coupled with a still-high fuel conversion (say a CO_2 yield higher than 90%). While this is usually the way to identify the achievement of MILD conditions with methane or natural gas, this is not enough with hydrogen-containing fuels, in particular when the fuel mixture contains a significant hydrogen amount, as for these experimental tests. As discussed by Derudi et al. [8,26], hydrogen-rich fuels, such as COG, are characterized by a smooth transition between flame and MILD conditions, with the absence of a sudden reduction of NO_x. Since the relevant issue of the MILD combustion process is a very low production of pollutants, a ''clean MILD'' condition has been considered, imposing to the criteria previously mentioned for the identification of MILD conditions an additional requirement concerning a maximum concentration of pollutants into the exhausts: NO_x below 30 ppm_v and CO below 50 ppm_v. For this reason, to point out when MILD combustion conditions are achieved while operating the burner with a hydrogen-containing fuel, the main pollutants emissions (NO_x and CO) are carefully monitored; all pollutants concentrations here reported are normalized on a dry basis and refer to average concentration values affected by a maximum discrepancy of ±7%.

3. Numerical model

The aforementioned experimental conditions have been simulated. In the first run the burner was fed with pure methane, whereas with a methane/hydrogen mixture (hydrogen content of 60% by vol.) in the other runs. For the runs with H_2, conditions with intermediate dilution factors were also investigated, since they experimentally led progressively to transition conditions and then to MILD regime (see Table 1).

The numerical model was developed with Fluent 6.3 by Ansys Inc.

The computational domain covers the combustion chamber so it is 0.33 m long with a radius of 0.025 m. The injection nozzle enters into the combustion chamber for 0.03 m.

A preliminary study was aimed at investigating the suitability of a 2-D model for the representation of the burner. Actually this was not clear, as the presence of 3 eccentric outlets at the top of the combustion chamber seemed to indicate that the computational domain should be made at least of a 120° angular sector of the combustion chamber. However, it was found that a 2-D model, realized with an annular outlet of area equivalent to the sum of those of the 3 eccentric outlets, leaded to results similar to those obtained with the 3-D model, being the maximum differences of predicted temperature across the burner lower than 10 K. This is because the reaction region is located rather far from the outlets sections, leading to uniform temperature and velocity distributions near them: consequently, the shape of the outlet section does not influence the temperature distribution in the combustion chamber. For this reason, a 2-D model was used

Table 1 – Summary of experimental and simulated runs.

Run	Mode	F_{CH4} [Nml/min]	F_{H2} [Nml/min]	$F_{H2}/(F_{H2}+F_{CH4})$ [%]	F_{AI} [Nml/min]	F_I [Nml/min]	F_{AII} [Nml/min]	T_{in} [K]
1	MILD	450.7	0	0	4574	0	0	1223
2	Flame	370.2	555.3	60	4411	0	582	1312
3	Transition	221.1	331.6	60	2981	2391	0	1312
4	Transition	221.1	331.6	60	2981	3271	0	1312
5	Transition	221.1	331.6	60	2981	4346	0	1312
6	MILD	221.1	331.6	60	2981	7606	0	1312

for all numerical simulations in order to reduce the computational time and make the simulations with detailed kinetics affordable.

Due to the structured type of the grid, a preliminary grid independency study was carried out on the 2-D domain through the Richardson extrapolation method [27]. The elements of the investigated grids were from 6 k to 26 k. The chosen grid was with 12 k elements and it ensured a grid convergence index (GCI) below 5% assuming as order of convergence $p=1$ and $p=2$ [28]. The actual order of convergence should be closer to 2, however, being all the simulations ran with second order of discretization.

Favre-averaged Navier–Stokes equations were solved by using the standard k–ε model to determine the Reynolds stress tensor. The radiative transfer equation was solved with the Discrete Ordinate technique with a number of directions solved equal to sixteen. The weighted sum of gray gases model (WSGG) with coefficients from Smith et al. [29] was used to evaluate the spectral properties of the participating medium.

3.1. *Turbulence/chemistry interaction*

Special attention was paid to the turbulence/chemistry interaction through the choice of the combustion model. In particular, the Eddy Dissipation/Finite Rate (ED/FR) model and the Eddy Dissipation Concept (EDC) were used as such models allow accounting for finite rate chemistry. Fast chemistry approaches (such as ED or Flamelet) were not considered as it is recognized that these are unsuited for MILD combustion [11,12].

According to the ED/FR model both a mixing rate, $\overline{w}_{k,ED}$, and an Arrhenius rate, $\overline{w}_{k,FR}$, based on the mean properties, are evaluated and the slower one is chosen as the mean reaction rate for the reacting species, i.e. $\overline{w}_k = \min(\overline{w}_{k,ED}, \overline{w}_{k,FR})$. However, the ED/FR model can handle only global kinetic mechanisms, being the turbulent rate the same for all the reactions.

Subsequently, the Eddy Dissipation Concept (EDC) [30] was used to take into account detailed chemistry. According to such a model, combustion occurs in the fine structures which are regions of the flow where the dissipation of turbulent kinetic energy takes place. Such regions are treated as perfectly stirred reactors (PSRs). A step-wise energy cascade model is used in EDC to evaluate the mass fraction of the fine structures, γ_λ:

$$\gamma_\lambda = 2.13\left(\frac{\nu\varepsilon}{\overline{k}^2}\right)^{1/4} \tag{6}$$

and the mean residence time of the fluid within them τ^*:

$$\tau^* = 0.41\left(\frac{\nu}{\varepsilon}\right)^{1/2} \tag{7}$$

In the above equations ν is the kinematic viscosity and ε is the dissipation of turbulent kinetic energy, k.

The mean source term in the conservation equation for the kth species is evaluated as:

$$\overline{w}_k = -\frac{\overline{\rho}\gamma_\lambda^2}{\tau^*}\frac{\left(\tilde{Y}_k - Y_k^*\right)}{\left(1-\gamma_\lambda^3\right)} \tag{8}$$

where $\overline{\rho}$ is the density of the mixture, Y_k^* is the mass fraction of the kth species in the fine structures and $\tilde{Y}_k$ represents the mean mass fraction of the kth species between the fine structures and the surrounding state. The value of $\tilde{Y}_k$ is obtained using:

$$\tilde{Y}_k = \gamma_\lambda^3 Y_k^* + \left(1-\gamma_\lambda^3\right)\, Y_k^0 \tag{9}$$

The EDC hypothesis is expected to provide satisfactory results for MILD combustion, as the system approaches perfectly stirred conditions due to the large flame dilution. Moreover, the effect of combustion process on turbulence is expected to be less significant than in a traditional flame, due to the flattening of the local gradients.

3.2. *Kinetic mechanisms*

Four different kinetic mechanisms were used to describe the oxidation of methane/hydrogen mixtures.

Global kinetic rates were applied with the ED/FR model for both CH_4 and H_2 [31]. When using the EDC model, the global reaction scheme was compared with detailed mechanisms. In particular three detailed mechanisms were used: the KEE-58 [31], the DRM-19 [32] and the GRI-3.0 w/o NO [33]. The KEE-58 mechanism consists of 18 species and 58 reactions. The DRM-19 mechanism is derived from the GRI-1.2 full mechanism [34], with the aim of defining the smallest set of reactions able to reproduce closely main combustion characteristics, i.e. ignition delays and laminar flame speeds. It consists of 19 species, plus Ar and N_2, for a total of 84 reversible reactions. The GRI-3.0 mechanism was used without the NO_x reactions resulting in 219 reversible reactions involving 36 chemical species.

3.3. *NO_x formation models*

As mentioned in the Introduction section, attention was focused on the modelling of NO_x formation paths.

The analysis of the thermal conditions of the burner (low temperatures and fluctuations) indicated that the NO thermal mechanism could be less important than other mechanisms, such as the N_2O intermediate route.

Thermal, prompt and N_2O routes were taken into account through models available in Fluent 6.3 [31]. All models are based on one-step kinetic mechanisms with Arrhenius equations integrated over a PDF for temperature in order to take into account the effect of turbulent fluctuations on the mean reaction rates.

As mentioned previously, the presence of H_2 in the fuel may promote NO formation through the NNH intermediate mechanism. Since such a mechanism is not available in the commercial CFD code, a bespoke subroutine (user-defined function written in C++ language) was coupled to the solver in order to consider NO formation through the NNH route according to the model suggested by Konnov [35]. In the model reaction of Eq. (1) is assumed to be equilibrated and NH (see Eq. (2)) is assumed to be fully converted into NO, leading to the following expression for the NO formation rate:

$$\frac{d[NO]}{dt} = 2k_2k_{p1}[N_2]\,[O]X_H \tag{10}$$

with the product of the rate constants of reaction of Eqs. (1) and (2) being $k_2k_{p1} = 2.5\times10^{-15}\exp(-3600/T)$ cm^3 mol^{-1} s^{-1}. In the above expression X_H is the mole fraction of H atoms.

Also in this case the turbulence–chemistry interaction was accounted for by integrating the rates with a PDF of the temperature.

It is worth noting that since the mechanism expressed by Eq. (10) needs the knowledge of the distribution of radicals such as O and H, it could be applied only to detailed kinetic mechanisms (KEE-58, DRM-19 and GRI-3.0).

3.4. Differential diffusion

Christo and Dally [12] showed that molecular diffusion played a significant role in the prediction of a jet of methane/hydrogen in hot coflow (JHC) simulating MILD combustion. Recently, Parente et al. [14] found negligible effects of molecular diffusion in the temperature predictions in a semi-industrial burner working promoting MILD regime through internal recirculation of exhaust gases. The authors concluded that the role of molecular diffusion is system dependent, thus it is largely affected by the way in which MILD combustion is achieved.

Consequently, it was chosen to include molecular diffusion in the present calculations, by calculating binary diffusion coefficients from the kinetic theory and a modification of the Chapman–Enskog formula [36]. Then, an effective diffusion coefficient of the species in the mixture was obtained by applying Wilke's mixing rule [37].

3.5. Boundary conditions

As far as the boundary conditions are concerned a mass flow rate with chemical species composition was given to the inlet section. It was also assumed the inlet gas temperature to be linearly dependent on the pre-heater nominal temperature, as experimentally verified. Resulting value of the inlet gas temperature is reported in the last column of Table 1. In flame conditions a mass flow rate was given to the secondary air inlet, whereas this was treated as a wall both for transition and MILD conditions.

Special attention needed the boundary conditions to be set at the combustion chamber wall. Its temperature was determined by identifying the value ensuring a flue gas temperature equal to the measured one. In other words, the wall temperature was set in order to satisfy the overall energy balance of the burner. As a result the wall temperature was found to be usually 100–150 K higher than the electric heater nominal temperature.

4. Results

The present section shows the main results provided by the CFD analysis of the lab-scale burner. Firstly, the main operating features of the system are discussed; then, a sensitivity analysis regarding the effect of the physical models (i.e. combustion model and pollutant formation route) on the results is carried out. The influence of the reactants dilution is also taken into account, investigating the transition of the system from flame to MILD regimes. Finally, the reliability of the proposed computational approach is supported by means of comparisons between experiments and numerical simulations.

4.1. Flow-field characterization

The numerical results (independently from the kinetic mechanism used in the turbulence/chemistry interaction model) indicate that the MILD conditions are ensured by both the internal recirculation of exhaust gases (due to their entrainment into the jet stream issuing in the combustion chamber) and the dilution of the feeding stream with nitrogen. In particular the numerical simulations can be exploited to characterize the different runs investigated in terms of aerodynamic recirculation ratio, R_A, which is needed to evaluate the dilution factor, k_v. The determination of R_A is not straightforward. In particular the calculation of the recirculated mass flow rate can be performed through the identification of the centers of the circulation loops and then integration of the radial profile of axial velocity from the center of the recirculation loop, $r = r_C$, to the walls, $r = R$:

$$R_A = \frac{2\pi \int_{r_C}^{R} \rho_E v_E(r) r \, dr}{\dot{m}_{AI} + \dot{m}_F + \dot{m}_{AII}} \tag{11}$$

The centers of the recirculation loops are determined as the points characterized by zero axial and radial velocities. The resulting values of R_A and k_v for the simulated runs are listed in Table 2, together with the location of the recirculation loop. It can be observed that the values of R_A are comprised between 5.3 and 6.1 for all the investigated runs, except for case 2, which has a larger R_A, i.e. 8.3, due to the presence of a secondary air inlet. However, the dilution factor, k_v, progressively increases when going from flame (Run 2, Table 2) to MILD (Run 6, Table 2), due to the effect of N_2 addition to the fuel stream.

4.2. Effect of turbulence/chemistry interaction models

The influence of turbulence/chemistry interaction models on the temperature distribution in the combustion chamber is firstly investigated.

Fig. 2 shows the temperature distribution inside the combustion chamber obtained with different combustion models and kinetic mechanisms, with the burner operating in MILD mode and fed with pure CH_4 (Run 1, Table 1). It can be noticed that the ED/FR model with one-step chemistry (Fig. 2a) predicts a high temperature reaction zone near the burner

Table 2 – Location of the center of the recirculation loop, aerodynamic recirculation ratio, R_A, and dilution factor, k_v, for the experimental runs investigated.

Run	Mode	x_C [m]	r_C [m]	R_A [–]	k_v [–]
1	MILD	0.087	0.014	5.3	5.3
2	Flame	0.100	0.014	8.3	7.3
3	Transition	0.090	0.014	6.1	10.6
4	Transition	0.089	0.014	5.6	11.2
5	Transition	0.090	0.014	5.6	13.2
6	MILD	0.091	0.014	5.7	19.1

nozzle, with a peak value of 1720 K. If the EDC model is employed with a one-step chemistry (Fig. 2b), the high temperature region disappears and a more uniform distribution is observed, with maximum temperatures of 1500 K. Therefore the turbulence/chemistry interaction treatment plays a major role in the determination of the combustion features. As far as the detailed mechanisms are concerned, the KEE-58 (Fig. 2c), DRM-19 (Fig. 2d) and GRI-3.0 (Fig. 2e) behave in a similar manner, maximum temperature being 1505 K, 1530 K and 1520 K, respectively. Fig. 3 shows the radial profiles of temperature at two axial locations along the axis, i.e. $x = 0.06$ m (a) and $x = 0.10$ m (b). Fig. 3 confirms that the ED/FR model and the simplified one-step chemistry approach result in higher temperatures in the region close to the axis, i.e. $r < 0.01$ m, whereas all profiles collapse onto a single line moving towards the walls, i.e. $r > 0.014$ m. This is expected since the recirculation loop generated by the incoming jet is located at a radius of approximately 0.014 m (Table 2) and, then, the temperature of the gases at radial coordinates larger than $r = 0.014$ m is that of the flue gases. Regarding the effect of the kinetic mechanism, Fig. 3b shows that the temperature profile provided by EDC with a one-step approach is flatter than those obtained with the detailed mechanisms, thus indicating that the oxidation process is already completed and the temperature distribution is uniform.

Fig. 4 shows the temperature distributions in MILD regime for the CH_4/H_2 mixture (Run 6, Table 1), obtained with different combustion models and kinetic mechanisms. It can be noticed that simple (2-step) kinetic mechanisms are strongly affected by hydrogen reactivity, resulting in an ignition region which is attached to the nozzle for the ED/FR case (Fig. 4a), and inside the injection pipe for the EDC case[1] (Fig. 4b). Conversely, the temperature distributions obtained with the reduced (Fig. 4c,d) and detailed mechanisms (Fig. 4e) denote the existence of a lifted and uniform reaction region, as one would expect when operating in MILD combustion regime.

To better investigate the sensitivity to the turbulence/chemistry interaction model and kinetic mechanism, radial profiles of temperature taken at different axial distances, i.e. $x = 0.06$ m and $x = 0.10$ m, are reported and compared in Fig. 5. The temperature values near the nozzle, $x = 0.06$ m (Fig. 5a) confirm that the global kinetic approach results in an early ignition of the fuel, for both ED/FR and EDC combustion models, temperatures along the axis are approximately 100 K higher than those predicted with the detailed kinetic schemes. As far as the detailed kinetic schemes are concerned, the temperature profiles obtained with KEE-58, DRM-19 and GRI-3.0 are in very good agreement at $x = 0.06$ m; small differences between DRM-19 and the other mechanisms are observed at $x = 0.10$ m. It should be recalled, however, that the DRM-19 mechanism has been developed for high temperature applications; at lower temperatures, as the ones investigated in the present study, the reduced mechanism is expected to be less accurate. Similarly to the methane case (Fig. 2), all the profiles tend to collapse onto a single line when increasing the radial distance from the axis, with the exception of the EDC model with 2-step scheme, which provides lower temperature levels. Such behaviour is confirmed at larger axial distances, $x = 0.10$ m (Fig. 5b), and can be ascribed to the partial ignition which takes place in the injection pipe resulting into lower temperature levels in the combustion chamber.

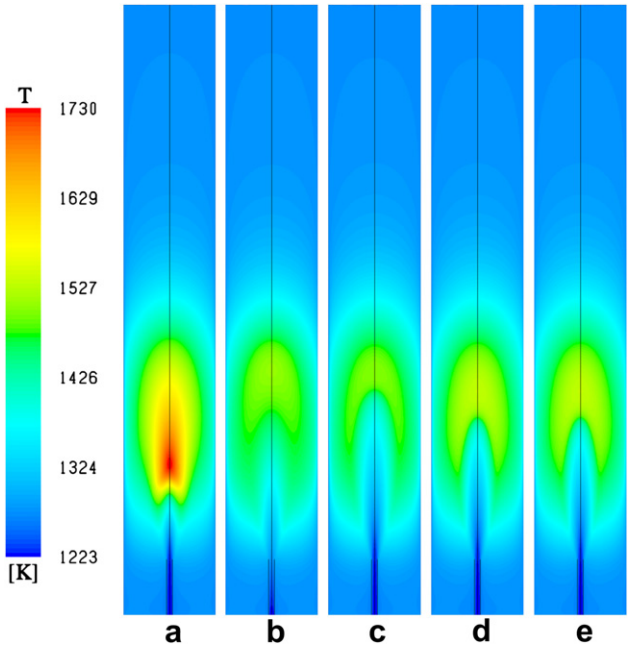

Fig. 2 – Temperature distribution in the burner fed with CH_4 in MILD combustion (Run 1, Table 1), predicted through: (a) ED/FR with 1-step mechanism, (b) EDC with 1-step mechanism, (c) EDC with KEE-58, (d) EDC with DRM-19, (e) EDC with GRI-3.0.

4.3. *Effect of dilution ratio on the combustion regime*

Fig. 6 shows the temperature distribution in the combustion chamber fed with the CH_4/H_2 mixture, predicted with EDC model and GRI-3.0 mechanism for different dilution ratios, k_v (that is, runs 2–6 in Table 2). The increase of k_v from 7.3 to 19.1 has been obtained, both experimentally and numerically by increasing the amount of nitrogen in the primary air. As mentioned previously, in flame conditions (Fig. 6a), secondary air at ambient temperature is also fed coaxially to the fuel jet, to stabilize the flame. These values of k_v have been experimentally found to involve flame ($k_v = 7.3$), transition ($k_v = 10.6$–13.2) and MILD ($k_v = 19.1$) conditions. It can be observed that the CFD simulations (carried out using particularly EDC model with GRI-3.0 mechanism) can qualitatively capture the transition from flame to MILD regimes. The maximum temperatures in the combustion chamber decrease dramatically with increasing k_v, from 2500 K for $k_v = 7.3$ (Fig. 6a), to approximately 1400 K, for $k_v = 19.1$ (Fig. 6e); this involves a reduction of the maximum temperature difference in the combustion chamber from about 2100 K to about 120 K. Moreover, the structure of the reaction zone is strongly affected by dilution: an attached flame is no longer observed above $k_v = 11.2$ (Fig. 6c) and the expansion of the high

[1] As a result of the ignition in the feeding pipe, the simulation carried out with EDC/2-step chemistry is extremely unstable. A fully converged solution was not obtained.

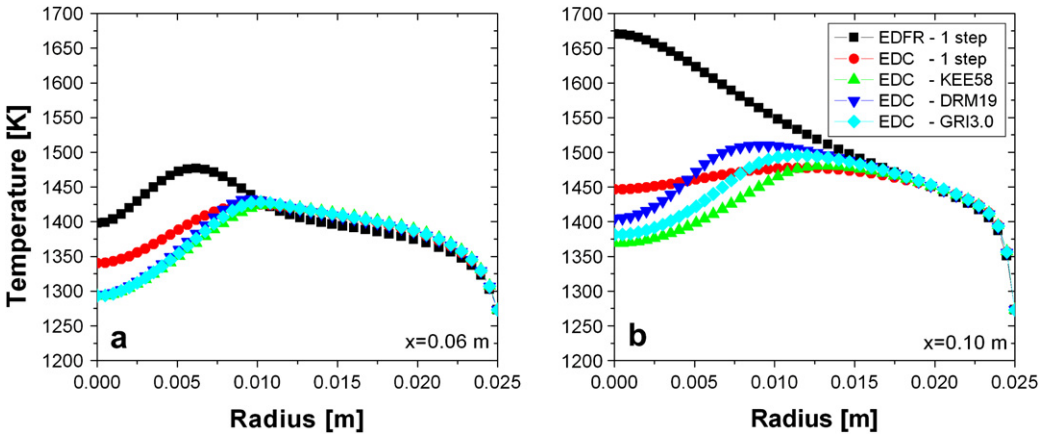

Fig. 3 – Radial profiles of temperature in the burner fed with CH_4 in MILD combustion (Run 1, Table 1) at different axial locations along the axis, i.e. $x = 0.06$ m (a) and $x = 0.10$ m (b), predicted by different combustion models and kinetic mechanisms.

temperature region to a large portion of the available volume in the combustion chamber is very clear.

Such considerations are also supported by the analysis of the temperature and OH mass fraction radial profiles at $x = 0.06$ m and $x = 0.10$ m, shown in Fig. 7. In particular, with regard to the OH radical mass fraction profiles (Fig. 7c,d), it can be observed that OH levels are much larger in flame regime, thus explaining the earlier ignition. Conversely, OH distribution is much more uniformly distributed in MILD regime, over a region whose extension is significantly larger than a traditional diffusive flame front, as shown out by Fig. 8.

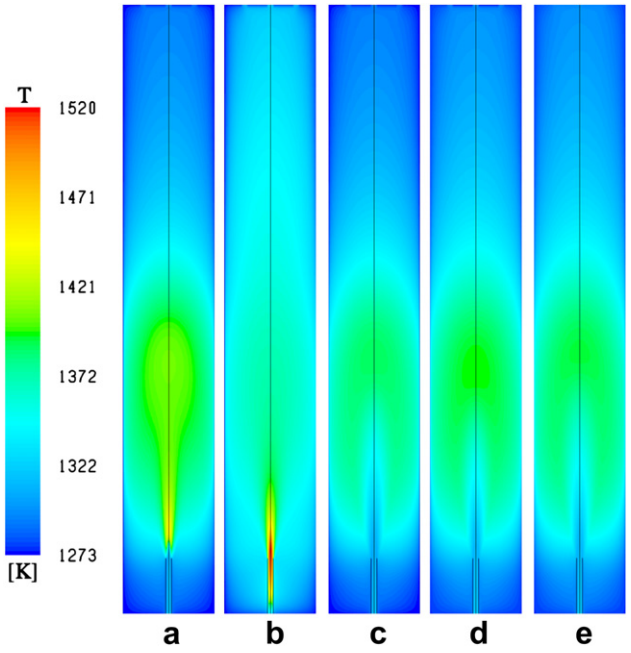

Fig. 4 – Temperature distribution in the burner fed with CH_4/H_2 mixture in MILD combustion (Run 6, Table 1), predicted through: (a) ED/FR with 1-step mechanism, (b) EDC with 1-step mechanism, (c) EDC with KEE-58, (d) EDC with DRM-19, (e) EDC with GRI-3.0.

4.4. *Model validation: comparison of experiments and simulations*

The validation of the numerical simulations is carried out by comparing the computational results with the experimental data in terms of both temperatures inside the combustion chamber and NO concentration in the outlet stream. No comparison is provided for the flue gas outlet temperature, as this value was used to tune the boundary condition at the walls.

4.4.1. *Temperatures*

Fig. 9 shows the comparison between the measured and calculated temperatures inside the combustion chamber at $x = 0.18$ m and $r = 0.014$ m (i.e. location denoted as "middle" location), for runs 2–6 of Table 1. The maximum experimental uncertainty is estimated as ± 50 K, especially in the regions of larger gradients. It can be observed that, with the exception of the ED/FR model, the predicted temperatures well represent the almost flat measured profile, although they slightly overpredict the temperature levels.

In order to quantitatively measuring the agreement between experimental data and computational predictions it was referred to metrics. In particular it was evaluated the average error metric normalized with respect to the measured value, $|\tilde{E}/\overline{y}_e|_{avg}$, which is defined as:

$$|\tilde{E}/\overline{y}_e|_{avg} = \left|\frac{y_m - \overline{y}_e}{\overline{y}_e}\right| \tag{12}$$

$\overline{y}_e$ and y_m are the mean measurement and the predicted value of variable y.

The third column of Table 3 lists the average error metrics $|\tilde{E}/\overline{y}_e|_{avg}$ calculated for temperatures at the same location considered in Fig. 9, i.e. middle location at $x = 0.18$ m and $r = 0.014$ m. With the exception of the ED/FR case, all the other models are characterized by an average error around 3%. It should be observed, however, that the measurements are taken at a radial position of 0.014 m, which corresponds approximately to the radial coordinate of the recirculation

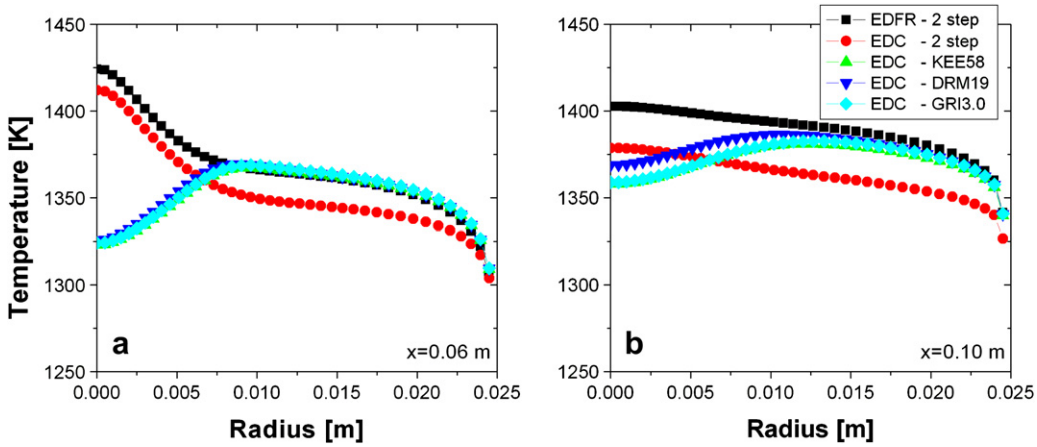

Fig. 5 – Radial profiles of temperature in the burner fed with CH_4/H_2 mixture in MILD combustion (Run 6, Table 1), at different axial locations along the axis, i.e. $x = 0.06$ m (a) and $x = 0.10$ m (b), predicted by different combustion models and kinetic mechanisms.

loop for all the simulated runs (see Table 2). Therefore, the monitored temperature is that of the flue gases, thus explaining the observed level of agreement of all models. Measurements taken inside the reacting fuel jet would certainly provide more useful information from the point of view of model validation, as they could capture the tendency of the global chemistry approaches to overpredict the temperature levels in the axis region.

The comparison between computed and measured temperatures is carried out for an additional position, $x = 0.10$ m, $r = 0.014$ m (i.e. "bottom" location) as shown by the second column in Table 3. Similar results to those obtained for position $x = 0.18$ m, $r = 0.014$ m are observed; however, larger discrepancies are found, due to the strong gradients which characterize the investigated zone.

From these results it could be concluded that the approach with EDC model and 2-step kinetic scheme is the best one for the description of the system. However, as discussed in the following this would determine unacceptable errors from the point of view of NO emissions.

4.4.2. *NO emissions*

Fig. 10 compares on a log-scale measured (black solid squares) and predicted NO emissions (empty symbols), for different

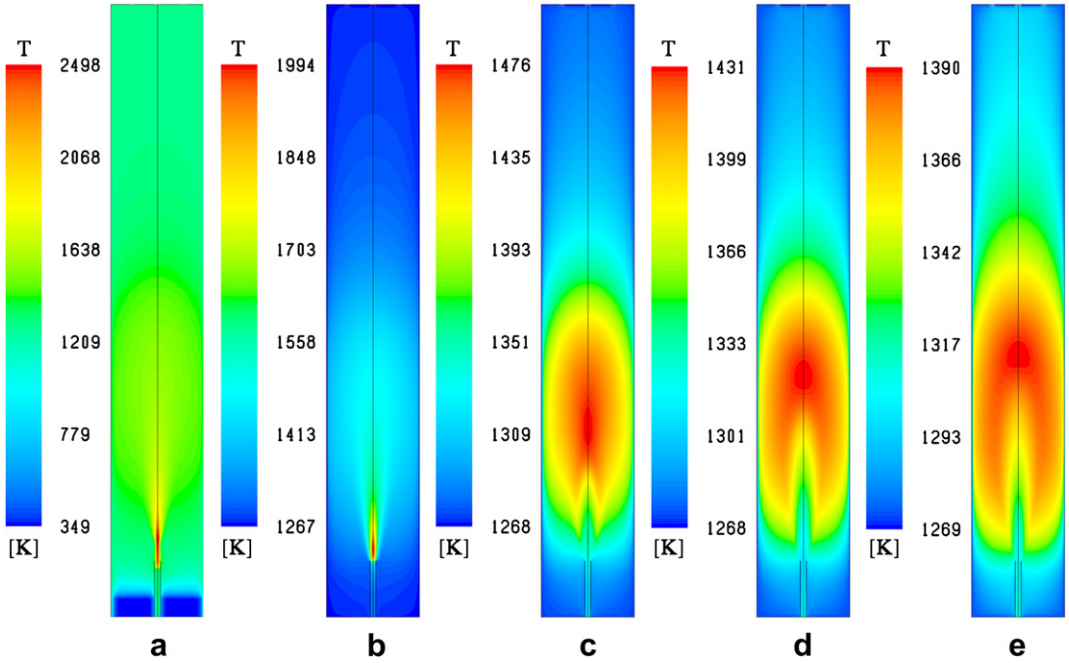

Fig. 6 – Temperature distribution into the burner fed with CH_4/H_2 mixture predicted by EDC with GRI-3.0 for different combustion conditions and dilution ratios, $k_v = 7.3$/flame (a), $k_v = 10.6$/transition (b), $k_v = 11.2$/transition (c), $k_v = 13.2$/transition (d) and $k_v = 19.1$/MILD (e) (Runs 2–6, Table 1).

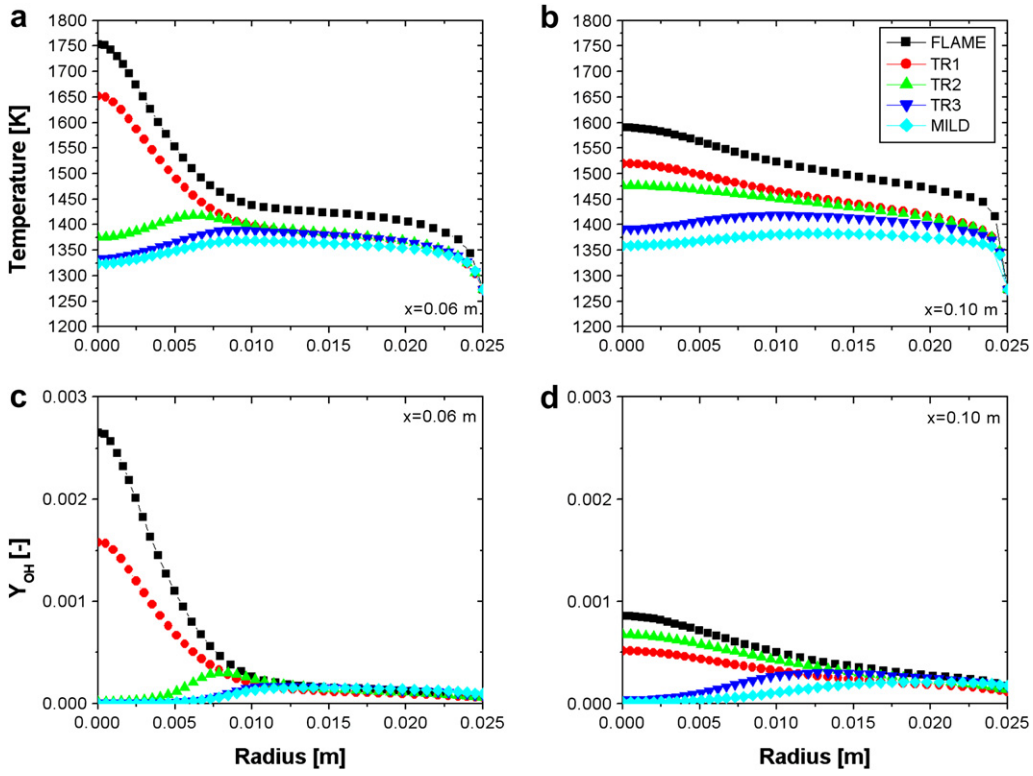

Fig. 7 – Radial profiles of temperature (a, b) and OH radical mass fraction (c, d) in the burner fed with CH_4/H_2 mixture at different axial locations along the axis, i.e. $x = 0.06$ m (a, c) and $x = 0.10$ m (b, d), predicted by EDC with GRI-3.0 for different dilution ratios, $k_v = 7.3$/flame (FLAME), $k_v = 10.6$/transition (TR1), $k_v = 11.2$/transition (TR2), $k_v = 13.2$/transition (TR3) and $k_v = 19.1$/MILD (MILD) (Runs 2–6, Table 1).

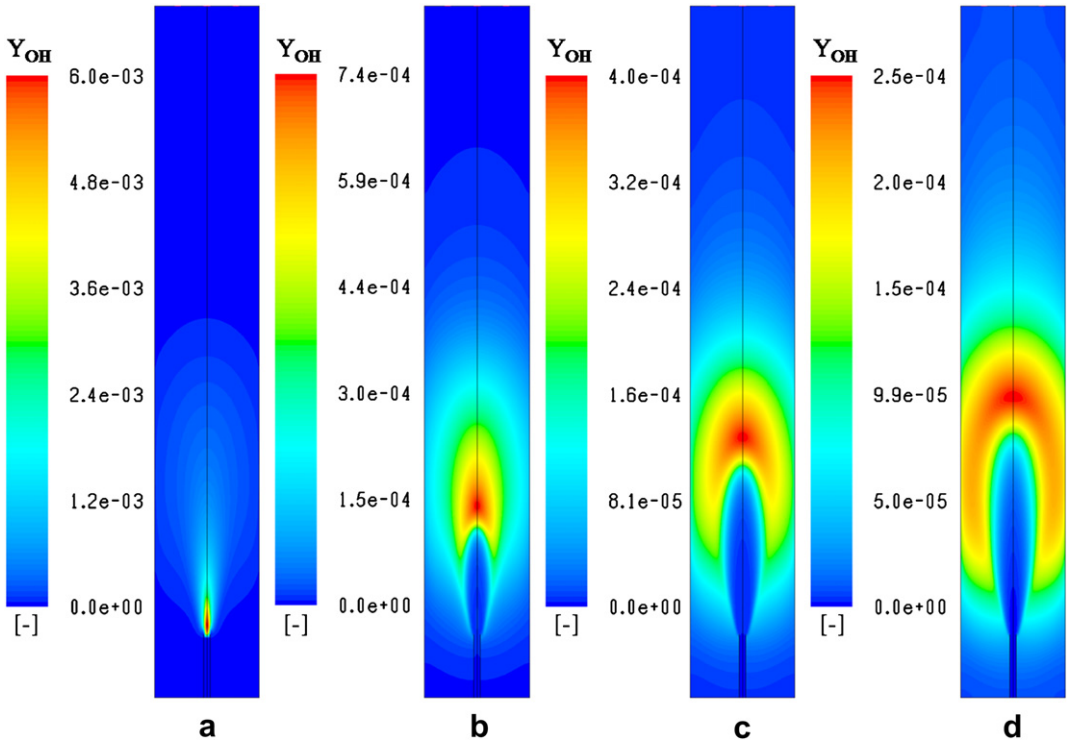

Fig. 8 – OH radical distribution in the burner fed with CH_4/H_2 mixture predicted by EDC with GRI-3.0 for different dilution ratios, $k_v = 10.6$/transition (a), $k_v = 11.2$/transition (b), $k_v = 13.2$/transition (c) and $k_v = 19.1$/MILD (d) (Runs 3–6, Table 1).

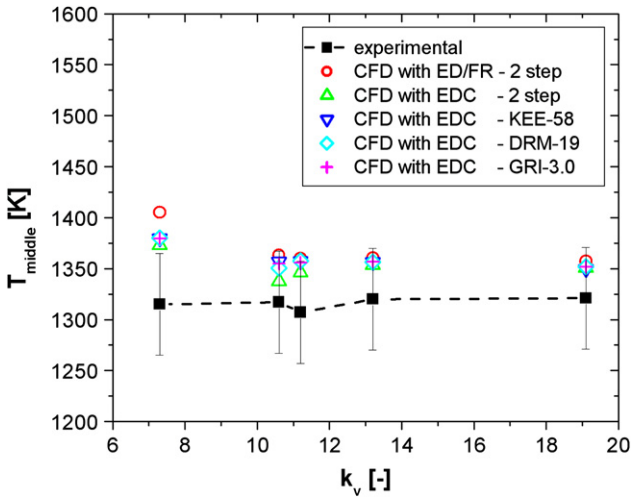

Fig. 9 – Comparison of measured and predicted temperatures (using different models) inside the burner at $x = 0.18$ m and $r = 0.014$ m, Runs 2–6, Table 1.

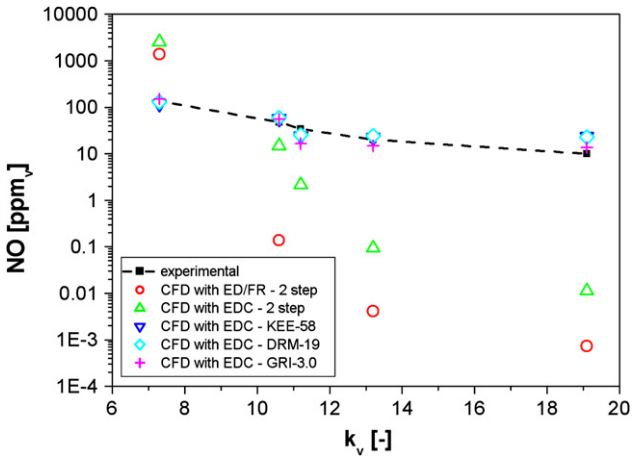

Fig. 10 – Comparison between measured and predicted NO emissions (dry basis) in the flue gases for the burner fed with CH_4/H_2 mixture for different dilution ratios, k_v. Temperature and species fields predicted by different combustion models and kinetic mechanisms. Runs 2–6, Table 1.

values of the dilution ratio, k_v, (runs 2–6 of Table 1). Predictions have been obtained from the temperature fields provided by different combustion models and kinetic mechanisms, by considering thermal, prompt, N_2O and NNH routes. The latter is only used in conjunction with reduced or detailed gas-phase mechanisms (KEE-58, DRM-19 and GRI-3.0) and not with the global mechanism since it requires the knowledge of H and O radical distributions.

In flame conditions ($k_v = 7.3$) a global kinetic approach (with both EDC and ED/FR) provides a temperature distribution which leads to overpredict the NO emissions by more than one order of magnitude. This is due to the large temperature peaks predicted by both ED/FR and EDC models with 2-step kinetic scheme, which strongly affect the thermal NO formation. Results obtained with reduced and detailed mechanisms (KEE-58, DRM-19 and GRI-3.0) are in good agreement each other and with the experimental evidences, being the maximum difference between measured and computed values equal to about 10%. An increase of k_v leads to a decrease of the measured NO, as expected in the transition from flame to MILD regimes. NO predictions obtained with reduced and detailed schemes are close to the experimental values, whereas simple global schemes predict NO levels at least one order of magnitude lower than the measured ones. This is mainly due to the fact that the NNH intermediate mechanism cannot be used with simplified chemistry approaches. Also in MILD conditions ($k_v = 19.1$) the measured NO value is close to the values predicted by GRI-3.0, KEE-58 and DRM-19. On the contrary EDC and ED/FR models with 2-step mechanism provide NO emissions at least three order of magnitude lower than the experimental value.

The average error metrics $|\tilde{E}/\overline{y}_e|_{avg}$ in Table 3 quantitatively confirm the aforementioned considerations. Global kinetic approaches, i.e. ED/FR and EDC with 2-step mechanism, result in very large error metrics, 265 and 426%, respectively. The predictions are strongly improved by employing a reduced kinetic mechanism (both KEE-58 and DRM-19 provide an average error metric of 41%). With a detailed mechanism

Table 3 – Average global validation metrics for temperature at two locations (bottom at $x = 0.10$ m and $r = 0.014$ m; and middle at $x = 0.18$ m, $r = 0.014$ m) and NO emission measurements.

Model	$\lvert\tilde{E}/\overline{y}_e\rvert_{avg}$		
	T_{bottom}	T_{middle}	NO
ED/FR – 2-step	0.07	0.04	2.65
EDC – 2-step	0.04	0.03	4.26
EDC – KEE-58	0.05	0.03	0.41
EDC – DRM-19	0.05	0.03	0.41
EDC – GRI-3.0	0.05	0.03	0.28

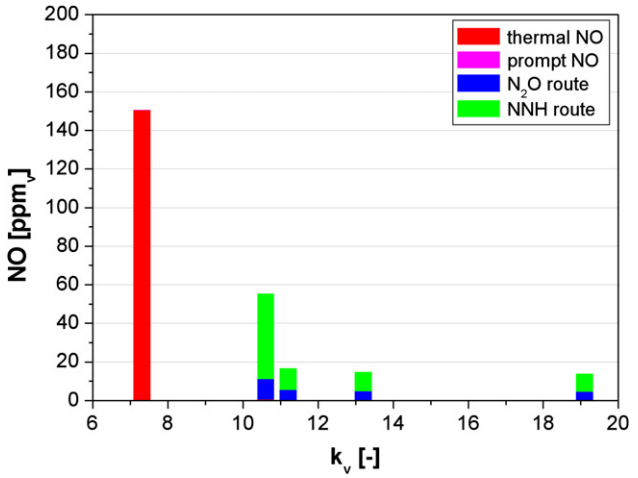

Fig. 11 – Contribution of different formation routes to the total NO emissions (dry basis) with CH_4/H_2 mixture for different dilution ratios, k_v. Temperature and species fields predicted by EDC with GRI-3.0. Runs 2–6, Table 1.

a further significant error reduction is achieved. The value of the average error metric provided by GRI-3.0, i.e. 28%, is quite satisfactory for the non-conventional conditions here investigated. Reaching a good predictivity for such small absolute values of NO emissions is very challenging for any modelling approach, since differences of even a few ppm_v lead to large relative errors when normalized to the measured values.

In order to better understand the role of the different formation routes on NO emissions, their contribution to the total NO is analyzed in Fig. 11 for different values of the dilution ratio, k_v. In flame regime, the thermal route is sufficient to explain the observed NO in the flue gases; however, when increasing the value of k_v, the thermal route becomes negligible and NO formation is dominated by NNH and N_2O pathways. Therefore, it appears clear that only the inclusion of these two mechanisms can allow a satisfactory prediction of NO emissions in MILD conditions when hydrogen-enriched fuels are involved.

5. Discussion and conclusions

A joint experimental and computational investigation of a lab-scale burner operating in MILD conditions and fed with hydrogen-enriched fuels showed that:

i) both the combustion model and the kinetic mechanism play an important role in determining the main combustion features, especially in presence of hydrogen. This is because hydrogen reactivity is usually overestimated by global kinetic approaches leading to unrealistic behaviours especially close to the reactants injection nozzle.
ii) The choice of the combustion model and kinetic mechanism is decisive for the determination of accurate temperature and chemical species fields, to be post-processed for NO emissions calculations (which are a primary task in MILD combustion modelling). With such a prerequisite, a reasonable agreement between predicted and measured NO can be obtained by means of simplified one-step approaches (integrated over probability density function of the temperature, to take into account turbulence effects), provided that all relevant NO formation routes at the investigated conditions are considered.
iii) Since the moderately low temperatures and low fluctuations of MILD combustion, Fenimore's prompt and the N_2O intermediate routes have to be included for NO calculations in addition to Zeldovich's thermal formation route.
iv) The NNH intermediate mechanism has also to be considered in presence of hydrogen. Since such a formation route is usually not available in commercial codes, it was implemented through a bespoke subroutine. In this manner it was found a good agreement between predicted and measured NO emissions which encourages further investigation.

Despite the difficulties related to the need of a proper turbulence/chemistry interaction treatment and rather detailed kinetic mechanisms for MILD combustion, the CFD model of the lab-scale device results to be very useful for the experimental activities, as for instance it allows evaluating the internal recirculation degree, a parameter which is otherwise difficult to be determined. Moreover it helps interpreting experimental evidences: for instance the CFD results indicated that the NNH and N_2O intermediate routes were the dominant formation pathways for the MILD conditions investigated in the present burner.

REFERENCES

[1] Cavaliere A, de Joannon M. Mild combustion. Prog Energy Combust Sci 2004;30:329–66.
[2] Dally BB, Riesmeier E, Peters N. Effect of fuel mixture on moderate and intense low oxygen dilution combustion. Combust Flame 2004;137:418–31.
[3] Wünning JA, Wünning JG. Flameless oxidation to reduce thermal NO-formation. Prog Energy Combust Sci 1997;23:81–94.
[4] Gupta AK. Thermal characteristics of gaseous fuel flames using high temperature air. J Eng Gas Turbines Power Trans ASME 2004;126:9–19.
[5] Choi GM, Katsuki M. Advanced low NO_x combustion using highly preheated air. Energy Convers Manage 2001;42:639–52.
[6] Effuggi A, Gelosa D, Derudi M, Rota R. Mild combustion of methane-derived fuel mixtures: natural gas and biogas. Combust Sci Technol 2008;180:481–93.
[7] Ilbas M, Crayford AP, Yılmaz I, Bowen PJ, Syred N. Laminar-burning velocities of hydrogen–air and hydrogen–methane–air mixtures: an experimental study. Int J Hydrogen Energy 2006; 31:1768–79.
[8] Derudi M, Villani A, Rota R. Mild combustion of industrial hydrogen-containing byproducts. Ind Eng Chem Res 2007;46: 6806–11.
[9] Yu Y, Gaofeng W, Qizhao L, Chengbiao M, Xianjun X. Flameless combustion for hydrogen containing fuels. Available at: http://dx.doi.org/10.1016/j.ijhydene.2009.04.036.
[10] Sabia P, de Joannon M, Fierro S, Tregrossi A, Cavaliere A. Hydrogen-enriched methane mild combustion in a well stirred reactor. Exp Therm Fluid Sci 2007;31:469–75.
[11] Coelho PJ, Peters N. Numerical simulation of a mild combustion burner. Combust Flame 2001;124:503–18.
[12] Christo FC, Dally BB. Modeling turbulent reacting jets issuing into a hot and diluted coflow. Combust Flame 2005;142:117–29.
[13] Galletti C, Parente A, Tognotti L. Numerical and experimental investigation of a mild combustion burner. Combust Flame 2007;151:649–64.
[14] Parente A, Galletti C, Tognotti L. Effect of the combustion model and kinetic mechanism on the mild combustion in an industrial burner fed with hydrogen enriched fuels. Int J Hydrogen Energy 2008;33:7553–64.
[15] Szegö GG, Dally BB, Nathan GJ. Scaling of NO_x emissions from a laboratory-scale mild combustion furnace. Combust Flame 2008;154:281–95.
[16] Bozzelli JW, Dean AM. NNH – a possible new route for NO_x formation in flames. Int J Chemical Kinetics 1995;27:1097–109.
[17] Hayhurst AN, Hutchinson EM. Evidence for a new way of producing NO via NNH in fuel-rich flames at atmospheric pressure. Combust Flame 1998;114:274–9.
[18] Konnov AA, Colson G, De Ruyck J. NO formation rates for hydrogen combustion in stirred reactors. Fuel 2001;80:49–65.
[19] Löffler G, Sieber R, Harasek M, Hofbauer H, Hauss R, Landauf J. NO_x formation in natural gas combustion: evaluation of simplified reaction schemes for CFD calculations. Fuel 2006;85:513–23.

[20] Rørtveit GJ, Hustad JE, Li SC, Williams FA. Effects of diluents on NO_x formation in hydrogen counterflow flames. Combust Flame 2002;130:48–61.
[21] Guo H, Smallwood GJ, Liu F, Ju Y, Gülder ÖL. The effect of hydrogen addition on flammability limit and NO_x emission in ultra-lean counterflow CH_4/air premixed flames. Proc Comb Inst 2005;30:303–11.
[22] Gauthier S, Nicolle A, Baillis D. Investigation of the flame structure and nitrogen oxides formation in lean porous premixed combustion of natural gas/hydrogen blends. Int J Hydrogen Energy 2008;33:4893–905.
[23] Glarborg P, Alzueta MU, Dam-Johansen K, Miller JA. Kinetic modelling of hydrocarbon/nitric oxide interactions in a flow reactor. Combust Flame 1998;115:1–27.
[24] Skottene M, Rian KE. A study of NO_x in hydrogen flames. Int J Hydrogen Energy 2007;32:3572–85.
[25] Cavigiolo A, Galbiati MA, Effuggi A, Gelosa D, Rota R. Mild combustion in a laboratory scale apparatus. Combust Sci Technol 2003;175:1347–67.
[26] Derudi M, Villani A, Rota R. Sustainability of mild combustion of hydrogen-containing hybrid fuels. Proc Comb Inst 2007;31:3393–400.
[27] Roache PJ. Verification and validation in computational science and engineering. Albuquerque, NM: Hermosa Publishers; 1998.
[28] Logan RW, Nitta CK. Comparing 10 methods for solution verification, and linking to model validation. J Aerospace Comput Inform Commun 2006;3:354–73.
[29] Smith F, Shen ZF, Friedman JN. Evaluation of coefficients for the weighted sum of gray gases model. J Heat Transfer 1982; 104:602–8.
[30] Magnussen BF. On the structure of turbulence and a generalized eddy dissipation concept for chemical reaction in turbulent flow. In: 19th AIAA aerospace science meeting, St. Louis, Missouri; 1981.
[31] Fluent 6.3 user guide.
[32] Kazakov A, Frenklach M. Reduced reaction sets based on GRI-Mech 1.2. Available at: http://www.me.berkeley.edu/drm/.
[33] Smith GP, Golden DM, Frenklach M, Moriarty NW, Eiteneer B, Goldenberg M, et al. GRI-3.0. Available at: http://www.me.berkeley.edu/gri_mech/.
[34] Frenklach M, Wang H, Yu C-L, Goldenberg M, Bowman CT, Hanson RK, et al. GRI-1.2. Available at: http://www.me.berkeley.edu/gri_mech/.
[35] Konnov AA, Colson G, De Ruyck J. The new route forming NO via NNH. Combust Flame 2000;121:548–50.
[36] McGee HA. Molecular engineering. New York: McGraw-Hill; 1991.
[37] Wilke SP. A viscosity equation for gas mixtures. J Comp Phys 1950;18:517–9.